CRYSTAL GROWTH & DESIGN

Article

pubs.acs.org/crystal

Controllable Fabrication of Coordination Polymer Particles (CPPs): A Bridge between Versatile Organic Building Blocks and Porous Copper-Based Inorganic Materials

Kuaibing Wang,[†] Zhirong Geng,[†] Mingbo Zheng,[‡] Luyao Ma,[‡] Xiaoyan Ma,[†] and Zhilin Wang*[,†]

[†]State Key Laboratory of Coordination Chemistry, School of Chemistry and Chemical Engineering, Nanjing University, Nanjing National Laboratory of Microstructures, Nanjing 210093, P. R. China

[‡]Nanjing National Laboratory of Microstructures, School of Electronic Science and Engineering, Nanjing University, Nanjing 210093, P. R. China

Supporting Information

ABSTRACT: Hierarchically micro-/nanostructured coordination polymer $[Cu(2,5\text{-PDC})H_2O]_n$ architectures with tunable morphologies have been successfully prepared by rationally adjusting the preparation parameters, such as the reactant concentration, solvent, surfactant, and reaction temperature. Using simple calcinations of chosen shaped $[Cu(2,5\text{-PDC})H_2O]_n$ architectures, we can obtain several porous copper-based inorganic motifs, which show potential applications for the antibacterial field and lithium ion batteries. Therein, CuO-1 can kill the Gram-positive bacteria *Bacillus subtilis and Staphylococcus aureus* better than other materials. The value for initial discharge capacity of CuO-3 (1160 mAh g^{-1}) is higher than the theoretical capacity (674 mAh g^{-1}) and most copper oxide materials. Besides, Cu/C composites also show intense application in the antibacterial and Li-ions uptake-release field, which will provide a widely used method to prepare the nanosystem of carbon-coating or carbon-compositing materials by simple calcinations of shaped precursor coordination polymer particles used under the proper temperature.

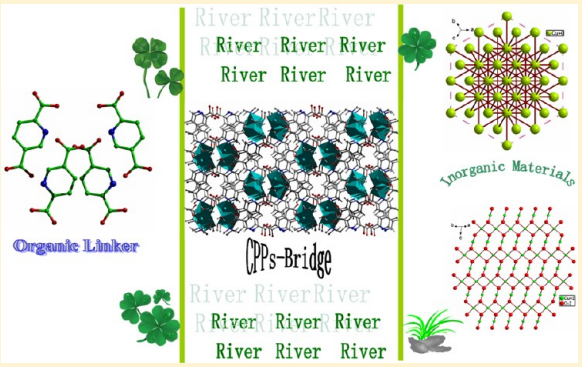

INTRODUCTION

Coordination polymer particles (CPPs), classified as crystalline metal−organic frameworks (MOFs)[1−3] and amorphous structures,[4−7] are a class of inorganic−organic hybrid materials formed by the assembly by metal ions and polydentate organic building blocks under mild contitions. CPPs possess potential advantages over other materials due to their structural tailorability and compositional diversity, allowing for the facile synthesis of micro-/nanostructures of different sizes, morphologies, and chemical properties.[8−12] Schematic transformation of CPPs to functional inorganic materials extends the roles of CPPs. Self-assembly involves choosing and designing versatile organic blocks with metal ions or clusters into shaped CPPs architectures, which can act as a precursors to form multifunctional inorganic products. Therefore, the CPPs can be regarded as stems to effectively connect a chemical family tree. It is necessary to point out that the simple transformations are significant for the following reasons: (i) Various shaped CPPs can easily be prepared by rationally adjusting synthetic systems under mild conditions, which can effectively transform to inorganic nanostructures with special architectures and multifunctional abilities; (ii) controlling the heating rate and calcining temperature of precursors can produce porous inner structures with fascinating properties; and (iii) CPPs play an important role in linking the kinds of organic materials with functional inorganic materials.

Copper oxide (CuO), as an important p-type transition-metal-oxide semiconductor with a narrow band gap (Eg = 1.2 eV), has been extensively studied for next generation rechargeable lithium-ion batteries due to their high theoretical capacity (674 mAh g^{-1}), low cost, and environmental benignity, etc.[13−15] However, there is still much room for progress with regard to the development of copper oxide micro-/nanostructures, particularly the synthesis of porous motifs and shape uniformity. Besides, porous Cu/C composites with well-defined morphologies are desired for many applications, such as catalysis, electrochemical capacitor response.[16,17] To date, alongside the development of nanotechnology, increased effort has been devoted to investigate the antibacterial properties of Cu/C materials.[18] The simple transformation of Cu-CPPs provides a practical exemplification to prepare porous copper−carbon materials. Moreover, nanomaterials of the carbon-coating or carbon-compositing system always show the incorporated function in controlled fashion and display

Received: August 6, 2012
Revised: September 9, 2012
Published: September 14, 2012

dx.doi.org/10.1021/cg3011234 | *Cryst. Growth Des.* 2012, 12, 5606−5614

enhanced performance. In this regard, considering the utilization of Cu/C nanocomposites in lithium-ion batteries, to the best of our knowledge, no studies address the Li-ions uptake-release abilities of Cu/C products. Herein, we report facile syntheses of various hierarchical $[Cu(2,5\text{-}PDC)H_2O]_n$ micro-/nanostructures with controllable morphologies by using coordination assembly between Cu^{2+} and the corresponding organic building blocks under changing correlated reaction parameters. A series of porous copper-based architectures were obtained by simple calcinations of several chosen shaped CPPs precursors under different experimental conditions. In addition, the antibacterial activities and Li uptake-release abilities of copper-based samples were also documented.

EXPERIMENTAL SECTION

Methods and Measurements. The antibacterial activities of the as-obtained copper-based products were tested against *Bacillus subtilis*, *Staphylococcus aureus*, *Alcaligenes faecalis*, *Pseudomonas aeruginosa*, *Proteus vulgaris*, and *Enterobacter cloacae* by determining the minimum inhibitory concentrations (MICs, $\mu g\ mL^{-1}$) through a colorimetric method using the dye 3-(4,5-dimethylthiazol-2-yl)-2,5-diphenyltetrazolium bromide (MTT).[3a,c] First, the stock solution of the synthesized samples (50 μg/mL) were prepared in dimethyl sulfoxide (DMSO), and graded quantities of the test crystals were incorporated in a specified quantity of sterilized liquid medium. Second, the solutions were poured into microtitration plates, and then a suspension of the microorganism with a concentration of approximately 10^5 cfu/mL was added. After incubation at 37 °C for 24 h, 50 μL of PBS (phosphate buffered saline 0.01 mol/L, pH 7.4: $Na_2HPO_4{\cdot}12H_2O$ 2.9 g, KH_2PO_4 0.2 g, NaCl 8.0 g, KCl 0.2 g, distilled water 1000 mL) containing 2 mg/mL of MTT was added to each well. Incubation was continued at room temperature for 4−5 h, followed by the addition of 100 μL of isopropanol containing 5% 1 mol/L HCl to extract the dye. At last, the optical density (OD) was measured with a microplate reader at 570 nm to determine the MICs.

To fabricate film electrodes, 80 wt % active material, 10 wt % carbon black, and 10 wt % polyvinyldifluoride (PVDF) binder were mixed into *N*-methylpyrrolidone (NMP). The obtained slurry was coated onto a copper foil current collector and then dried in vacuum. Coin cell was assembled in an argon-filled glovebox with the MIO/GNS nanocomposite as the working electrode, Li metal foil as the counter electrode, 1 M LiPF6 in ethylene carbonate and diethyl carbonate (EC/DMC, 1:1 vol) as electrolyte, and Celgard 2250 as separator. Charge−discharge measurements were carried out galvanostatically at various current densities over a voltage range of 0.01−3 V (vs Li/Li^+) using a battery test system (LAND, Wuhan Jinnuo Electronics Ltd.).

X-ray powder diffraction (XRPD) data were collected on a Bruker D8 Advance instrument using Cu Kα radiation (λ = 1.54056 Å) at room temperature. The morphology of the as-prepared samples and the corresponding energy dispersive X-ray (EDX) spectroscopy were obtained by using a Hitachi S-4800 field-emission scanning electron microscope (FE-SEM). Transmission electron microscopy (TEM) images were captured on the JEM-2100 instrument microscopy at an acceleration voltage of 200 kV. The adsorption isotherm of nitrogen was measured at 77 K by using Micromeritics ASAP 2020 M+C volumetric adsorption equipment. Electrospray ionization mass spectrometry (ESI-MS) measurements were performed with an LCQ fleet mass spectrometer. The nucleation process was monitored by a 90Plus Particle analyzer (Brookhaven Instruments Corporation). All inorganic samples were (4 mg) separately dispersed in the media (4 mL) used to grow bacteria to shake for 12 h, and then the copper ion released from the corresponding samples were tested using an optical emission spectrometer (OES, Optima 5300 DV, PerkinElmer).

Synthesis of CPPs. The building blocks pyridine-2,5-dicarboxylic acid (2,5-H_2PDC) and NaOH with the molar ratio of 1:2 were dissolved in deionized water to form 0.1 M 2,5-Na_2PDC aqueous solution. In a typical synthesis of $[Cu(2,5\text{-}PDC)H_2O]_n$ architectures, 0.1 M $Cu(OAc)_2$ aqueous solution was introduced into 0.1 M 2,5-Na_2PDC aqueous solution drop by drop in mixed solvents (water/ethanol: 10/10, v:v) or pure deionized water (20 mL) under vigorous stirring, and a large amount of blue precipitate occurred immediately. After the sample was stirred for 20 min, the precipitate was collected by centrifugation, and washed several times with ethanol and water. The different shaped $[Cu(2,5\text{-}PDC)H_2O]_n$ samples were carried out by adjusting the synthetic parameters, such as concentrations, solvents, the amount of polyvinylpyrrolidone (PVP K30, M = 58000) and sodium dodecyl sulfonate (SDS), and temperature (R.T. and 80 °C), while other reaction conditions were kept unchanged. Notably, the surfactant was first dissolved in the solvent, and then the reactants were added. The higher temperature reaction was carried out by a refluxing method under vigorous stirring.

Synthesis of Cu-Based Materials. The chosen shaped precursors were first dispersed in ethanol and dried in 35 °C for 4 h in a porcelain combustion vessel. For preparation CuO nanostructures, the precursors were heated in air to 450 °C and maintained for 30 min, while Cu/C composites were obtained by calcining the precursors under Ar atmosphere at 450 °C for 30 min. The heating rate of the furnace was kept at 1 °C/min.

RESULTS AND DISCUSSION

In a typical experiment, copper acetate acting as the metal source, which is more suitable for control through the coordination modulation,[19] reacted with the bridging linker 2,5-H_2PDC to obtain several coordination polymer morphologies under different reaction environments. In the present system, the synthetic parameters, such as the reactant concentration, solvent, surfactant, and reaction temperature play important roles in controlling the morphology and size of the coordination compound. The resulting morphology and size evolution under different reaction conditions is summarized in Table S1. First of all, the concentration of reactants used in the reaction system was found to be a vital factor for manipulating the morphology and size of the resulting samples. S1−S3 coordination polymer species were prepared at different concentrations in binary solution as depicted in Figure 1. The morphology varied gradually from square-like to oval-lump-like as the concentration increased, respectively. As shown in Figure 1a,b, the four sides of the square were curved not straight, and the square-like architectures with the thickness about 160 nm were obtained on a large scale. As concentration continued increasing, the shelled-melon-seed-like motifs with a mean thickness of 250 nm were formed as clearly seen in Figure 1c,d. Notably, there is a cuspate cap in the one side of a single motif, which looks like shelled melon seeds (Figure 1d), so we called the microstructures "shelled-melon-seed architectures". The low-magnification SEM image (Figure 1e) shows a typical image of the as-synthesized oval-lump-like particles by introducing the solution (0.4 mmol) into the 2,5-Na_2PDC solution (0.4 mmol) under stirring treatment at room temperature. From the enlarged SEM image shown in Figure 1f, the thickness of the polymer sample was about 800 nm, and both terminals of the microstructures were flat, not sharp as that of so-called shelled-melon-seed particles. In addition, the edge of oval-lump looks like paring into several planes with a knife. The formation of the hierarchical motifs is considered to be a crystal splitting process.[20] Thus, the concentration of reactants does have an effect on the size and shape of the final products, and tunable morphologies of above-mentioned can be achieved in a convenient manner.

Second, besides concentration, the solvent used also can influence the morphology and size of the resulting products. The pure solvent (water) was used in the reaction system, keeping the same concentration gradient, and samples of S4−

dx.doi.org/10.1021/cg3011234 | Cryst. Growth Des. 2012, 12, 5606−5614

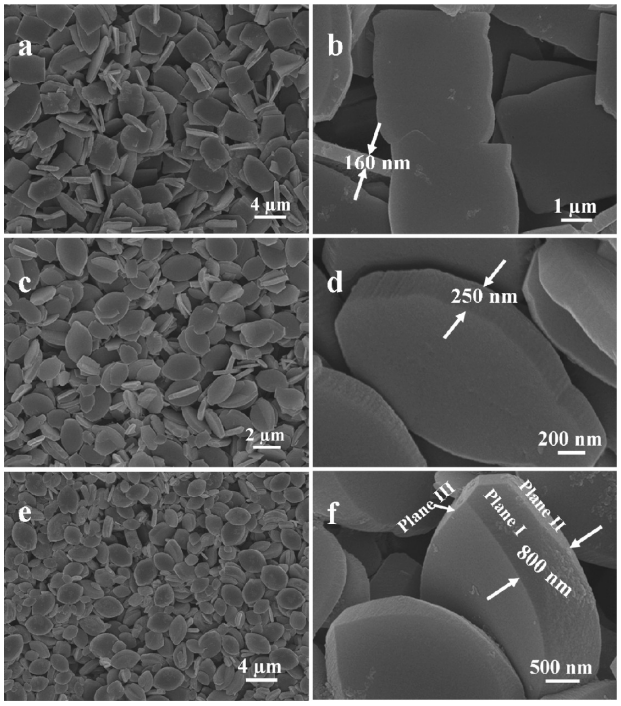

Figure 1. (a, b) SEM images of square-like morphology. (c, d) SEM images of shelled-melon-seed-like motifs. (e, f) SEM images of oval-lump-like morphology.

S6 can be obtained as illustrated in Figure 2. At lower concentration, dispersive capped spindle-like particles were generated with an average length and thickness of 2 μm and 100 nm, respectively (Figure 2a,b). Notably, the height of the flat cap was about 50 nm as closely seen in Figure 2b. With the

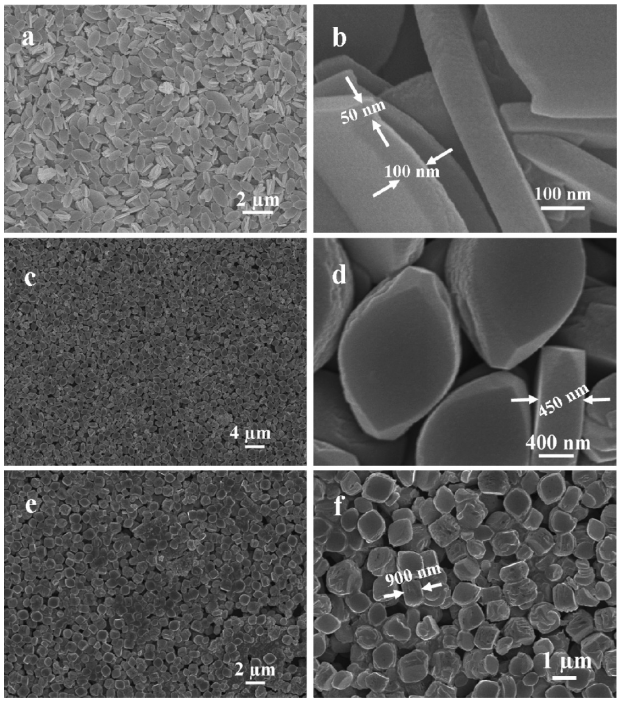

Figure 2. (a, b) SEM images of capped spindle-like morphology. (c, d) SEM images of eye-like motifs. (e, f) SEM images thicker eye-like morphology. S4–S6 was prepared at different concentrations in water.

concentration increased, lots of uniform eye-like products with a mean thickness of 450 nm were formed as shown in Figure 2c,d. Notably, it is different from the sample S3 due to their more regular and uniform oval-lump shape. However, at higher concentration, the as-formed products were not dispersed well, which have rough surfaces with a mean thickness of 900 nm (Figure 2e,f). In light of this observation, the different polarity of solvent can lead to different assembly and stacking modes of Cu-carboxylate metal–organic frameworks, because the change of dipole–dipole interactions would induce different kinetic control and initial speciation.

Recently, sodium dodecyl sulfonate (SDS) and polyvinyl pyrrolidone (PVP), as two kinds of surfactants, have been widely used to control nucleation and crystallization of well-defined materials with special orientation and morphology in most solution reactions.[20] Thus, we investigated the amounts of two surfactants influencing the morphology evolution under two different solvents system (mixed solvents and water) by fixing the same molar ratio of reactants (0.2:0.2 mmol). First, when the amount of PVP varied from 0.05 to 0.5 g, samples of S7–S10 and S11–S14 were obtained in the mixed solvents and pure water reaction system, respectively. As summarized in Figure 3, the size of the as-obtained products were larger and thicker with the increase of mass of PVP, and the dual motifs gradually disappeared and the morphology grew into rounded-lump at the highest amount of PVP (0.5 g). Take S10 and S14 for example (Figure 3, panels d and h): they both show the

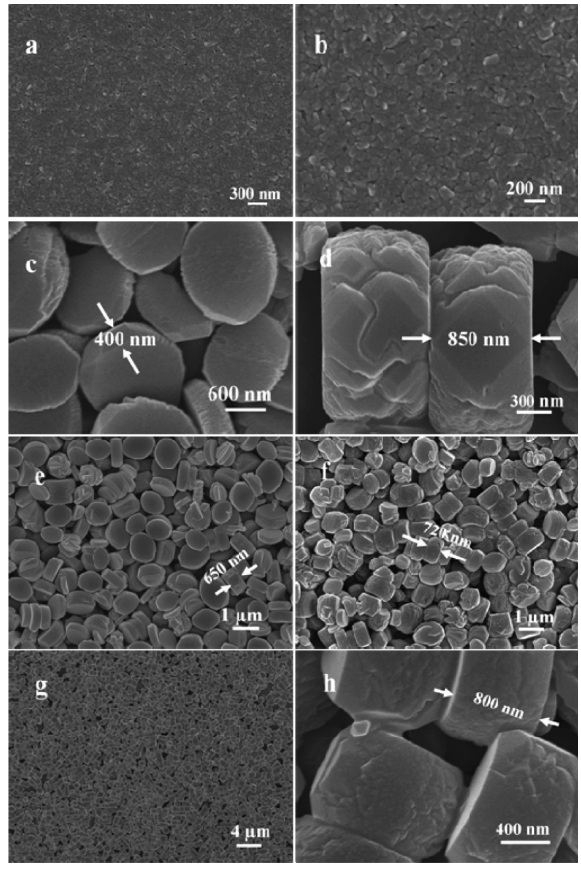

Figure 3. (a–d) SEM images of $[Cu(2,5\text{-}PDC)H_2O]_n$ architectures in mixed solvents with different amounts of PVP (0.05 g, 0.1 g, 0.2 and 0.5 g). (e and h) SEM images of $[Cu(2,5\text{-}PDC)H_2O]_n$ architectures in pure water with different amounts of PVP (0.05 g, 0.1 g, 0.2 and 0.5 g).

dx.doi.org/10.1021/cg3011234 | *Cryst. Growth Des.* 2012, 12, 5606–5614

rounded-lump shape with a similar thickness of 800 nm, while the difference between them is the rough degree on the surface. On the one hand, it indicates the PVP effect on the resulting morphology evolution. On the other hand, it also shows the influence of solvent polarity. Meanwhile, SDS influences on the morphology evolution under identical conditions are illustrated in Figure S1−S2 (see Supporting Information (SI)). Samples of S15−S22 were generated on a large scale with a shiny surface. In addition, in mixed solvents, the morphology changes a lot, while a smaller evolution happens in pure water. Besides, under higher amounts of SDS in the water system, the samples stick together, not showing apparent shapes at a glance. We think that is a suggestion of the excessive addition of SDS. On the basis of the above observations, we can assume that the surfactants may play a vital role in the resulting morphology and size of products. Herein, the surfactants may benefit from the oriented nucleation, and lower energy cost for creating new surfaces, and thus affecting the morphology evolution of Cu-based coordination polymers.

By keeping other conditions unchanged (details see Table S1), the effect of system temperature on the size and shape of as-prepared products was investigated. Samples S23 and S24 were obtained at 80 °C by refluxing for 20 min as illustrated in Figure 4. They both display a drum-like shape with widths of

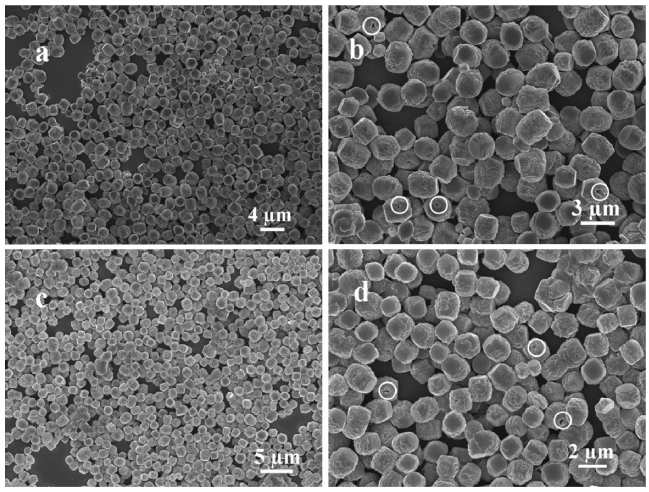

Figure 4. (a, b) SEM images of drum-like morphology (PVP: 0.1 g, 80 °C, refluxing). (c, d) SEM images of similar drum-like morphology (SDS: 0.1 g, 80 °C, refluxing).

1−2 μm and thicknesses of 2−3 μm. It is found that small amounts of different surfactants have no apparent influence on the resulting morphology. The morphology character is a single drum particle has been bulged in the middle, with the top and down remaining thin while the dual patterns remain flat. Detailed SEM analysis reveals that the middle part of drum-like crystals has a fissure on it, looking like a bursting belly in the process of crystal growth (see the circle in Figure 4, panels b and d). Generally speaking, at a higher temperature, there will appear a large number of nuclei after supersaturating, which will lead to slow growth, and thus forming the drum-like metal−organic architectures on a large scale. The possible growth mechanism of the CPPs at different temperatures was clearly depicted in Scheme 1.

The chemical composition and crystal structure of the above-mentioned samples were detected by X-ray powder diffraction (XRD) measurements. As shown in Figure 5a, all observed peaks can be indexed to the bulk phase $[Cu(2,5\text{-PDC})H_2O]_n$,[21] indicating that the as-obtained samples under different experimental conditions are isostructural. As to the crystal structure of $[Cu(2,5\text{-PDC})H_2O]_n$ molecules, the 2,5-H_2PDC ligand bridging two Cu ions to form a 3D network structure with the aid of noncovalent interactions as depicted in Figure 5b,c. Therefore, the above 3D microstructures and crystal structure suggest that the formation of the obtained samples is attributed to coordination-induced assembly from copper ions and 2,5-H_2PDC building blocks in polar solvent.[22]

In particular, the simple calcinations of the unusually shaped coordination polymer particles resulting in inorganic materials (metal oxides and metals) extend the roles of inorganic−organic hybrid materials.[23] Herein, we obtained Cu-based inorganic products (CuO or Cu/C nanostructures) by calcinations of chosen drum-like, spindle-like, and rounded-lump samples in air or Ar, namely, CuO-1, CuO-2, CuO-3, Cu/C-1, Cu/C-2, and Cu/C-3, respectively. Typically, the above shaped CPPs were simply calcined under air at 450 °C for 30 min using a conventional furnace to obtain copper oxide (CuO) nanostructures. The morphology of CuO products was characterized by SEM as vividly shown in Figure 6. The overall sizes of CuO samples were decreased, while the unique morphologies were maintained as compared with the initial precursors (Figure 6a,c,e). Detailed enlarged SEM analysis shows that the single CuO-1 sample which has a cavity center is gathered by a large number of nanoparticles. The size of these particles is in the range of 40−50 nm as seen in Figure 6b. Similarly, CuO-2 and CuO-3 samples are also comprised of lots of particles with a mean diameter of 40 nm (Figure 6d,f). The X-ray diffraction (XRD) pattern shown in Figure 7a confirms the formation of monoclinic copper oxide (JCPDS 05-0661). All observed peaks can indexed to the reported pure bulk CuO.

Scheme 1. The Possible Growth Mechanism of CPPs at R.T. and 80 °C, respectively

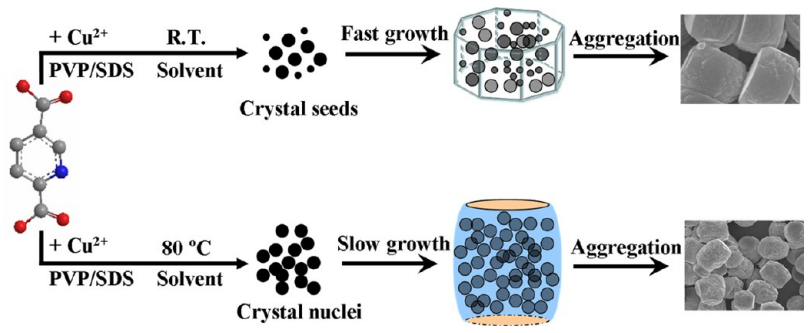

dx.doi.org/10.1021/cg3011234 | Cryst. Growth Des. 2012, 12, 5606−5614

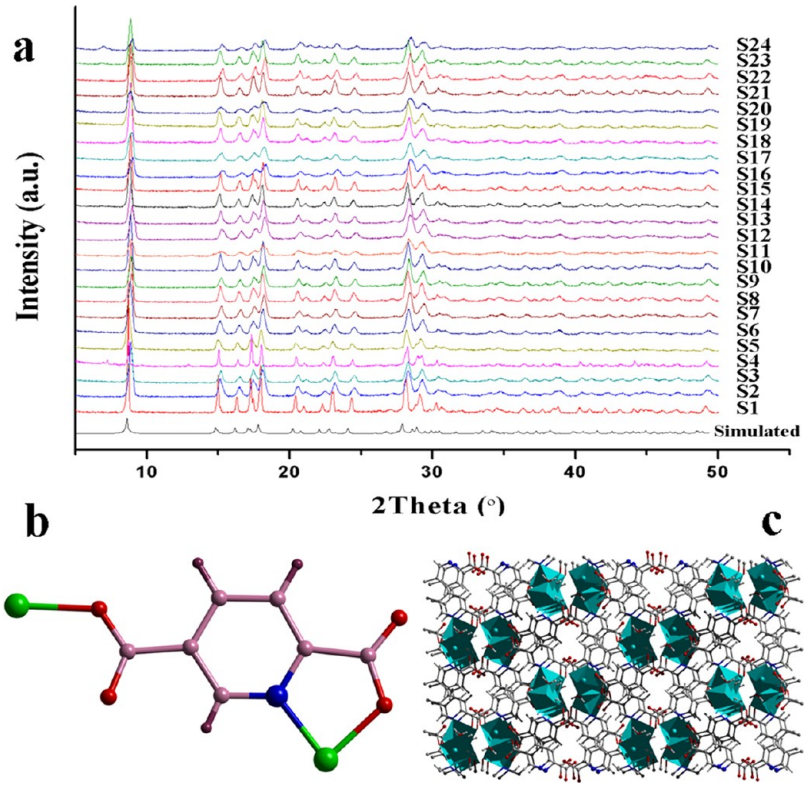

Figure 5. (a) A simulated XRD curve based on the bulk phase of $[Cu(2,5\text{-PDC})H_2O]_n$ molecules and XRD patterns of as-synthesized samples. (b) Coordination modes of carboxylate groups. (c) 3D network of $[Cu(2,5\text{-PDC})H_2O]_n$ architectures.

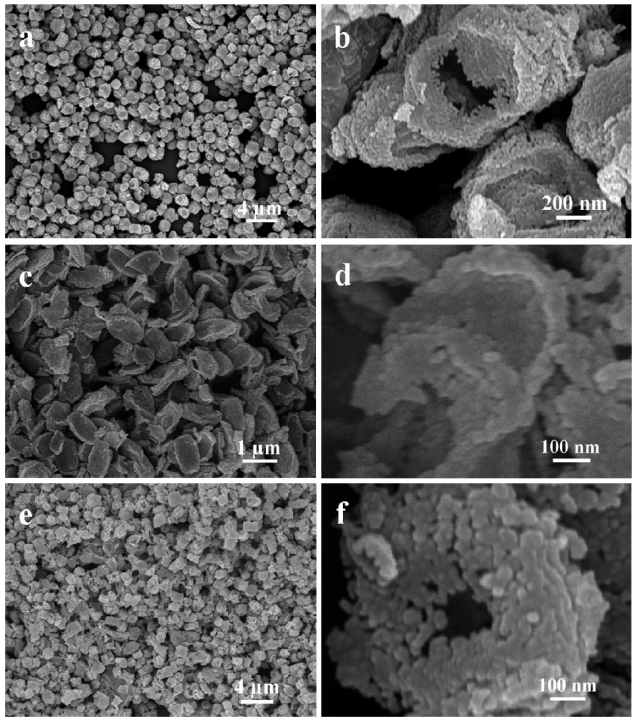

Figure 6. SEM images of CuO-1 (a, b), CuO-2 (c, d), and CuO-3 (e, f) at different magnifications.

Obviously, the characteristic peaks attributed to (110), ($\bar{1}$11), and (111) in as-synthesized CuO samples showing different remarkably intensities in comparison with those in simulated CuO patterns, reveals that the as-obtained CuO samples prefer to grow along these crystal planes. When the precursors calcined under Ar atmosphere at 450 °C for 30 min, another copper-based nanostructure, Cu/C composite structures, can be generated. The chemical compositions of as-obtained Cu/C composite samples were characterized by energy dispersive X-ray spectroscopy (EDX, Figure S3 in Supporting Information), by which only copper and carbon atoms were detected. Furthermore, the XRD pattern of these products can be indexed as the cubic phase of Cu (JCPDS No. 04-0836) (Figure 7b). The carbon arose from the 2,5-PDC linker, and Cu^{2+} was reduced to Cu by the carbon at 450 °C in Ar atmosphere. Cu/C-1 displays a rod-like shape with an average diameter of 200 nm, and looks like splitting upon original precursor's shape (drum-like morphology) in the process of calcinations (Figure 8a,b). Cu/C-2 inherits the shape as compared with the precursor as shown in Figure 8c. Differently, the image of TEM (Figure 8d) shows the Cu/C-2 sample has a porous inner structure and the overall size was reduced in comparison with the precursor. Similarly, the Cu/C-3 sample inherits the morphology while it possesses a smaller size when compared with the original precursors. The center of a single rounded-lump was cracked and the mean thickness after calcination was around 450 nm as depicted in Figure 8e,f. The above results show that the as-prepared copper-based samples all display special morphologies (especially porous inner structures, Figure S4 shows the mesoporous cavity distributions of representive samples of CuO-1 and Cu/C-1, around 20 nm) and sizes, which would make them viable candidates for potential applications in biomaterials and lithium ions batteries.

On the basis of the above observations, the structural schematic diagram on formation processes of the corresponding Cu-based products is summarized in Scheme 2. First, the organic building blocks coordinating with metal ions to form crystal seeds, and then these seeds increase a lot with the

dx.doi.org/10.1021/cg3011234 | Cryst. Growth Des. 2012, 12, 5606−5614

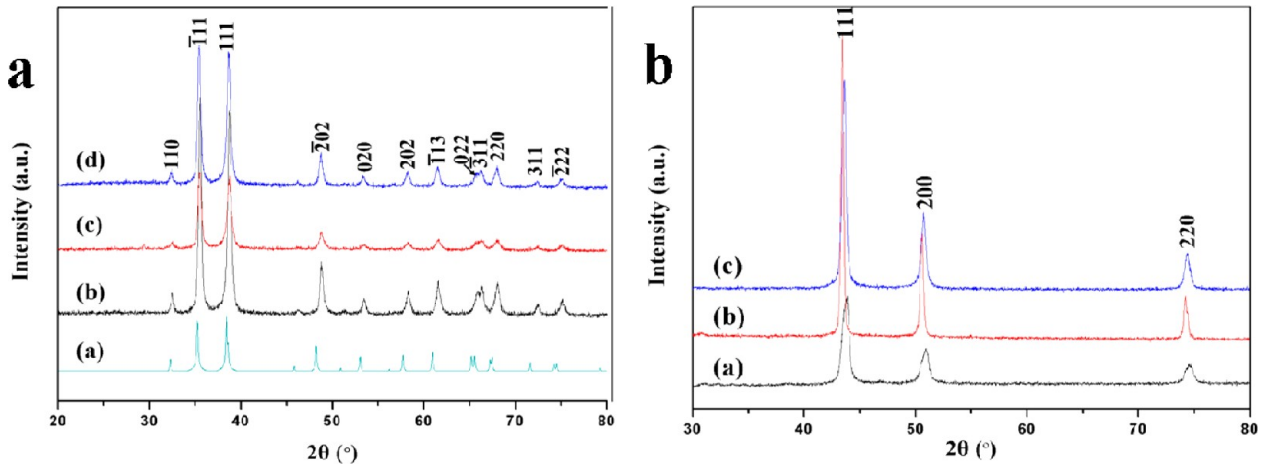

Figure 7. (a) A simulated XRD curve based on the bulk phase of CuO and XRD patterns of as-synthesized CuO samples. (b) XRD patterns of as-synthesized Cu samples.

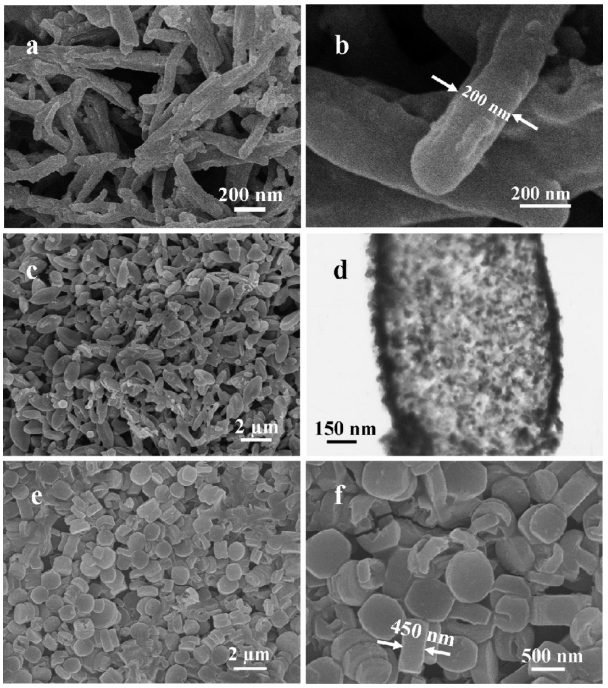

Figure 8. SEM images of Cu/C-1 (a, b), Cu/C-2 (c), and Cu/C-3 (e, f) at different magnifications. (d) TEM image of porous Cu/C-2 sample.

Scheme 2. The Formation Process of Cu-Based Polymers and Inorganic Materials

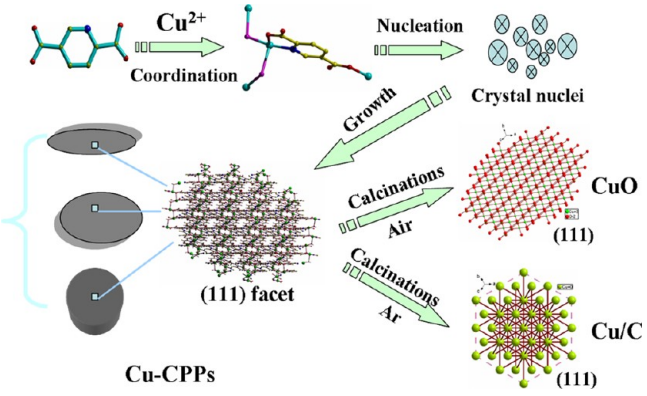

growth and aggregation process to obtain the Cu-based CPPs. Notably, the reaction rate is so fast that forming the coordination polymer immediately when metal ions adding into the solution containing organic linker. The possible process before forming crystal seeds were monitored by ESI-MS as shown in Figure S5. Furthermore, the nucleation process was detected by Particle Analyzer at room temperature. As demonstrated in Figure S6, we monitored the reaction time from 1 to 10 min when the reaction started, and the result illustrated that it did obtain lots of crystal seeds in different sizes and consequently formed the Cu-based CPPs in micrometer regime. Second, calcinations of the shaped CPPs precursors under different conditions can gain porous Cu-based inorganic materials. It is noteworthy that the reason for generating a series of porous structures is releasing lots of exhaust gases in the calcinations process. Interestingly, seen from the crystal structures, the coordination number of the copper center ion changes from 5 to 4 in the calcining process of $[Cu(2,5\text{-}PDC)H_2O]_n$ to Cu; however, in the reduction process to Cu/C materials, the coordination number of Cu increases to 12. At a higher temperature, $[Cu(2,5\text{-}PDC)H_2O]_n$ molecules decompose, and Cu^{2+} is easy to coordinate with the O_2 to form CuO and is apt to obtain Cu by the reduction of carbon. The coordination number is probably concerned with the coordination geometry optimization. Additionally, viewing along the (111) crystal plane of Cu-based products, they all display the hexahedral motifs. The results indicate that the calcinations of CPPs into inorganic materials may occur along a certain direction or crystal plane.

The reduction of particle size and the diversity nanostructures should make copper-based materials show different functionalities. Herein, we first studied the antimicrobial activities of the resulting copper-based products against Gram positive (*B. subtilis* and *S. aureus*) and Gram negative bacteria (*Salmonella enteriditis*, *Escherichia coli*, *P. vulgaris*, and *P. aeruginosa*) by determining the minimum inhibitory concentrations (MIC) through a colorimetric method using the dye MTT. The examined results are presented in Table 1, and verify that all samples have a certain bacteriostatic ability to some of tested six bacteria. Clearly seen from Table 1, it is obvious that all products except Cu/C-3 show more intense antibacterial activities against Gram-positive bacteria than

dx.doi.org/10.1021/cg3011234 | *Cryst. Growth Des.* 2012, 12, 5606−5614

Table 1. MICs (Minimum Inhibitory Concentrations) (μg mL^{-1}) of As-Synthesized Copper-Based Products

	minimum inhibitory concentration/μg mL^{-1}					
	Gram positive		Gram negative			
samples	*B. subtilis*	*S. aureus*	*S. enteriditis*	*E. cloacae*	*P. vulgaris*	*P. aeruginosa*
CuO-1	6.25	6.25	6.25	50	25	25
CuO-2	12.5	12.5	12.5	>50	25	50
CuO-3	12.5	25	25	>50	25	25
Cu/C-1	6.25	12.5	12.5	50	50	25
Cu/C-2	12.5	25	25	>50	25	25
Cu/C-3	50	50	50	>50	50	50

against Gram-negative bacteria. Therein, CuO-1 and Cu/C-1 show high antimicrobial abilities against *B. subtilis*, *S. aureus*, and *S. enteriditis*, illustrating a certain antibacterial selectivity of copper-based materials. On one hand, the possible reason for analyzing the above results may be certain morphologies exposing certain crystal faces dissolve faster and have thus a stronger metal ion release than others, and consequently have different antibacterial activities. The result shows that the antibacterial abilities was in correlation with the Cu-ion released from the corresponding inorganic samples, which is in good agreement with OES data examined as listed in Table 2. On the

Table 2. Cu-Ion Releasing from the Different Samples in the Media Were Measured by OES

samples	Cu^{2+} (mg/L)
CuO-1	262.85
CuO-2	220.32
CuO-3	142.02
Cu/C-1	245.75
Cu/C-2	170.17
Cu/C-3	95.57
media used to grow bacteria	0.005

other hand, the N_2 adsorption−desorption isotherms were measured to evaluate the specific surface area of copper-based nanostructures. As shown in Figure S7, the specific surface area for Cu/C-1 is larger than that of other two Cu/C composites, leading to intense antimicrobial activity. Notably, the similar surface area of CuO samples resulting in different antibacterial abilities may demonstrate that the composition and the special nanostructures of nanosystems might be the other reason for explaining the different bacteriostatic abilities.

To demonstrate the potential application of as-prepared copper-based materials with high electronic conductivity, galvanostatic discharge curves for Cu-based materials/Li cells were recorded at a current density of 200 mA g^{-1} for the first discharge cycle as depicted in Figure 9a. The initial discharge capacity of CuO-1, CuO-2, and CuO-3 electrodes was about 742, 784, and 1160 mAh g^{-1}, respectively. These values were larger than the theoretical capacity of 674 mAh g^{-1} and other reported CuO samples based on a maximum uptake of 2Li/CuO.[24] The improvement may be attributed to the following reasons. First, the hierarchical porous inner structures can be regarded as three-dimensional (3D) current collector motifs, which shorten the diffusion length and provide negligible diffusion time, and consequently improve the electrochemical performance. Second, the hierarchical porous inner structures may also be considered as a flexible buffer to relieve the strain associated with about a 174% volume expansion of CuO during Li^+ uptake (CuO converts to Cu and Li_2O), restrain particle pulverization and sustain electronic contact, and thus guarantees good power performance.[25] The initial discharge capacity that exceeds the nominal capacity can be attributed to the decomposition of the electrolyte and subsequent formation of the solid electrolyte interphase layer and organic conductive polymer on the CuO surface that occurs in the low potential region. In addition, the initial formation of lithium oxide and the presence of some residual OH^- groups in the active CuO samples are also responsible for the additional discharge capacity.[26] Meanwhile, Cu/C composites were also investigated under identical treatments. The Cu/C composite materials showing the performance of Li uptake-release abilities are completely ascribed to carbon materials allowing it to exceed the stoichiometric limit of Li-ion intercalation.[27] From Figure 9a, the initial discharge capacity of Cu/C-1, Cu/C-2, and Cu/C-3 electrodes was 534, 386, and 478 mAh g^{-1}, respectively, which were larger than that of commercial graphite (372 mAh g^{-1}). Therefore, although Cu is inactive to lithium, as a current collector, it enhances electronic conductivity and thus improves the performance of Li uptake-release abilities for carbon materials. To the best of our knowledge, this is the first time

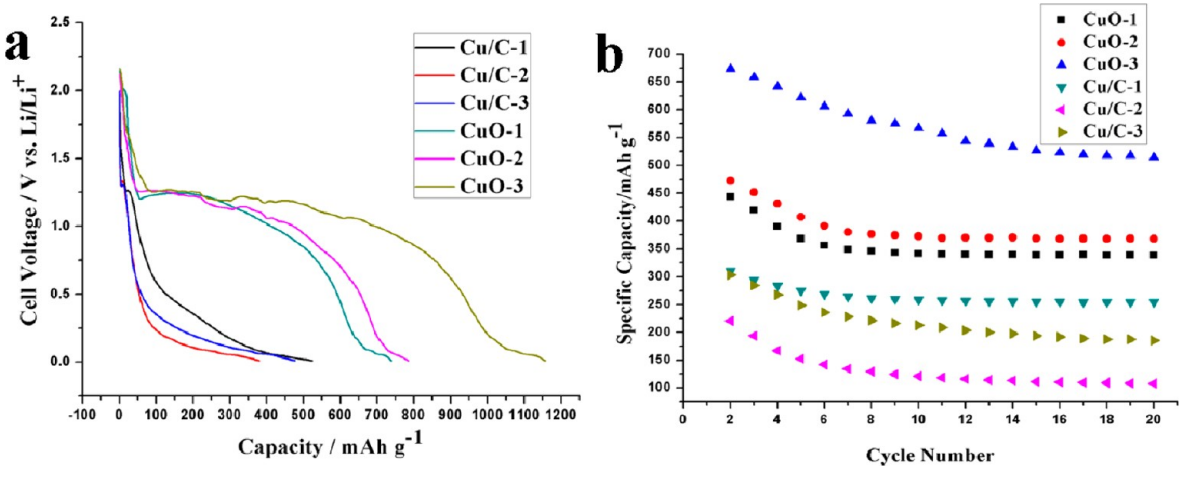

Figure 9. (a) The initial discharge curves of copper-based materials. (b) Cycling profile of electrodes made of copper-based nanoparticles at a current density of 200 mA g^{-1} for 2−20 cycles.

dx.doi.org/10.1021/cg3011234 | *Cryst. Growth Des.* 2012, 12, 5606−5614

that Cu/C composites were used in the field of lithium ion batteries. The simple calcinations from shaped CPPs to porous inorganic materials may provide an effective way to produce carbon-coating materials for solving long-time cycling problem in Li-ion batteries. Cycling performance of the copper-based samples electrode at a current density of 200 mA g^{-1} is shown in Figure 9b. It is evident that the above electrodes exhibit high capacities and display outstanding chemical/mechanical robustness. Therefore, the application of these low-cost and high-performance hierarchical copper-based micro-/nanostructures for lithium ion batteries is feasible and promising.

CONCLUSION

In summary, a simple and straightforward method to prepare and control the morphology of CPPs by adjusting the corresponding reaction parameters has been presented. Hierarchical porous copper-based products can be obtained by easy calcinations of these precursor CPPs used. Therein, the shaped Cu-CPPs can be regarded as a bridge to connect the O,N-bifunctional organic building blocks 2,5-H_2PDC with diverse copper-based materials, which will provide a practical and new paradigm in the manufacture of functional inorganic micro-/nanostructures. That is, by choosing proper organic linker and designing synthetic parameters, inorganic nano-systems will be obtained through simple calcinations of shaped CPPs. In addition, the as-obtained copper-based products with special architectures show intense antibacterial properties and display enhanced performances in Li-ion storage.

ASSOCIATED CONTENT

Supporting Information

Table for different morphologies under the corresponding experimental parameters, SEM images for adding different amounts of SDS, EDX patterns for Cu/C materials, and N_2 adsorption−desorption isotherms of Cu-based materials. This material is available free of charge via Internet at http://pubs.acs.org.

AUTHOR INFORMATION

Corresponding Author

*Tel: +86-25-83686082. Fax: +86-25-83686082. E-mail: wangzl@nju.edu.cn.

Notes

The authors declare no competing financial interest.

ACKNOWLEDGMENTS

This work was supported by the National Natural Science Foundation of China (21075064, 21027013, 21021062 and 21275072) and the National Basic Research Program of China (2013CB922102).

REFERENCES

(1) (a) Tanaka, D.; Henke, A.; Albrecht, K.; Moeller, M.; Nakagawa, K.; Kitagawa, S.; Groll, J. *Nat. Chem.* **2010**, *2*, 410−416. (b) Cho, W.; Lee, H. J.; Oh, M. *J. Am. Chem. Soc.* **2008**, *130*, 16943−16946. (c) Yaghi, O. M.; O'Keeffe, M.; Ockwig, N. W.; Chae, H. K.; Eddaoudi, M.; Kim, J. *Nature* **2003**, *423*, 705−714.

(2) (a) Diring, S.; Furukawa, S.; Takashima, Y.; Tsuruoka, T.; Kitagawa, S. *Chem. Mater.* **2010**, *22*, 4531−4538. (b) Ma, J.; Jiang, F. L.; Chen, L.; Wu, M. Y.; Zhang, S. Q.; Han, D.; Feng, R.; Hong, M. C. *Cryst. Growth Des.* **2011**, *11*, 3273−3281. (c) Rowsell, J. R. C.; Yaghi, O. M. *Angew. Chem., Int. Ed.* **2005**, *44*, 4670−4679.

(3) (a) Wang, K. B.; Yin, Y. X.; Li, C. Y.; Geng, Z. R.; Wang, Z. L. *CrystEngComm.* **2011**, *13*, 6231−6236. (b) Du, M.; Zhang, Z. H.; Tang, L. F.; Wang, X. G.; Zhao, X. J.; Batten, S. R. *Chem.—Eur. J.* **2007**, *13*, 2578−2586. (c) Wang, K. B.; Geng, Z. R.; Yin, Y. X.; Ma, X. Y.; Wang, Z. L. *CrystEngComm* **2011**, *13*, 5100−5104. (d) Horcajada, P.; Serre, C.; Vallet-Regí, M.; Sebban, M.; Taulelle, F.; Férey, G. *Angew. Chem., Int. Ed.* **2006**, *45*, 5974−5978.

(4) (a) Spokoyny, A. M.; Kim, D.; Sumrein, A.; Mirkin, C. A. *Chem. Soc. Rev.* **2009**, *38*, 1218−1227. (b) Wang, K. B.; Ma, X. Y.; Shao, D. L.; Geng, Z. R.; Zhang, Z. Y.; Wang, Z. L. *Cryst. Growth Des.* **2012**, *12*, 3786−3791.

(5) Cho, W.; Lee, Y. H.; Lee, H. J.; Oh, M. *Chem. Commun.* **2009**, 4756−4758.

(6) Oh, M.; Mirkin, C. A. *Nature* **2005**, *438*, 651−654.

(7) Shi, H. Y.; Deng, B.; Zhong, S. L.; Wang, L.; Xu, A. W. *J. Mater. Chem.* **2011**, *21*, 12309−12315.

(8) (a) Rocca, J. D.; Liu, D. M.; Lin, W. B. *Acc. Chem. Res.* **2011**, *44*, 957−968. (b) Imaz, I.; Hernando, J.; Ruiz-Molina, D.; Maspoch, D. *Angew. Chem., Int. Ed.* **2009**, *48*, 2325−2329. (c) Horcajada, P.; Chalati, T.; Serre, C.; Gillet, B.; Sebrie, C.; Baati, T.; Eubank, J. T.; Heurtaux, D.; Clayette, P.; Kreuz, C.; Chang, J.-S.; Hwang, Y. K.; Marsaud, V.; Bories, P.-N.; Cynober, L.; Gil, S.; Férey, G.; Couvreur, P.; Gref, R. *Nat. Mater.* **2010**, *9*, 172−178.

(9) (a) Cho, W.; Lee, Y. H.; Lee, H. J.; Oh, M. *Adv. Mater.* **2011**, *23*, 1720−1723. (b) Jeon, Y.-M.; Armatas, G. S.; Heo, J.; Kanatzidis, M. G.; Mirkin, C. A. *Adv. Mater.* **2008**, *20*, 2105−2110. (c) Rieter, W. J.; Taylor, K. M. L.; An, H.; Lin, W.; Lin, W. *J. Am. Chem. Soc.* **2006**, *128*, 9024−9025. (d) Lee, H. J.; Cho, W.; Oh, M. *CrystEngComm* **2010**, *12*, 3959−3963.

(10) (a) Sun, X.; Dong, S.; Wang, E. *J. Am. Chem. Soc.* **2005**, *127*, 13102−13103. (b) Lu, W.; Chui, S. S.-Y.; Ng, K.-M.; Che, C. M. *Angew. Chem., Int. Ed.* **2008**, *47*, 4568−4572. (c) Ni, Z.; Masel, R. I. *J. Am. Chem. Soc.* **2006**, *128*, 12394−12395. (d) Liu, K.; You, H.; Jia, G.; Zheng, Y.; Song, Y.; Yang, M.; Huang, Y.; Zhang, H. *Cryst. Growth Des.* **2009**, *9*, 3519−3524.

(11) (a) Jo, C.; Lee, H. J.; Oh, M. *Adv. Mater.* **2011**, *23*, 1716−1719. (b) Tsuruoka, T.; Furukawa, S.; Takashima, Y.; Yoshida, K.; Isoda, S.; Kitagawa, S. *Angew. Chem., Int. Ed.* **2009**, *48*, 1−6. (c) Imaz, I.; Martínez, M. R-; Fernández, L. G-.; García, F.; Molina, D. R-.; Hernando, J.; Puntes, V.; Maspoch, D. *ChemComm.* **2010**, 4737−4739. (d) Jung, S.; Oh, M. *Angew. Chem., Int. Ed.* **2008**, *47*, 2049−2051. (e) Carné, A.; Carbonell, C.; Imaz, I.; Maspoch, D. *Chem. Soc. Rev.* **2011**, *40*, 291−305.

(12) (a) Jeon, Y.-M.; Armatas, G. S.; Kim, D.; Kanatzidis, M. G.; Mirkin, C. A. *Small* **2009**, *5*, 46−50. (b) Chifotides, H. T.; Dunbar, K. R. *Acc. Chem. Res.* **2005**, *38*, 146−156. (c) Xin, Z.; Bai, J.; Shen, Y.; Pan, Y. *Cryst. Growth Des.* **2010**, *10*, 2451−2454. (d) Dang, S.; Liu, Q.; Liu, K.; Guo, Z.; Sun, L.; Song, S.; Zhang, H. *Cryst. Growth Des.* **2010**, *10*, 4662−4667.

(13) Jiao, F.; Bruce, P. G. *Adv. Mater.* **2007**, *19*, 657−660.

(14) Zhang, W.; Li, M.; Wang, Q.; Chen, G.; Kong, M.; Yang, Z.; Mann, S. *Adv. Funct. Mater.* **2011**, *21*, 3516−3523.

(15) Bruce, P. G.; Scrosati, B.; Tarascon, J. -M. *Angew. Chem., Int. Ed.* **2008**, *47*, 2930−2946.

(16) Ju, Y. W.; Choi, G. R.; Jung, H. R.; Kim, C.; Yang, K. S.; Lee, W. J. *J. Electrochem. Soc.* **2007**, *154*, A192−A197.

(17) Shi, Q. H.; Liang, H. J.; Feng, D.; Wang, J. F.; Stucky, G. D. *J. Am. Chem. Soc.* **2008**, *130*, 5034−5035.

(18) Gao, F.; Pang, H.; Xu, S.; Lu, Q. *Chem. Commun.* **2009**, 3571−3573.

(19) Farha, O. K.; Spokoyny, Y. M.; Mulfort, K. L.; Galli, S.; Hupp, J. T.; Mirkin, C. A. *Small* **2009**, *5*, 1727−1731.

(20) Liu, K.; You, H.; Jia, G.; Zheng, Y.; Huang, Y.; Song, Y.; Yang, M.; Zhang, L.; Zhang, H. *Cryst. Growth Des.* **2010**, *10*, 790−797.

(21) Min, D.; Yoon, S. S.; Jung, D.-Y.; Lee, C. Y.; Kim, Y.; Han, W. S.; Lee, S. W. *Inorg. Chem. Acta* **2001**, *324*, 293−299.

(22) Weng, W.; Li, Z.; Jamieson, A. M.; Rowan, S. J. *Macromolecules* **2009**, *42*, 236−246.

(23) (a) Foster, P. M.; Burbank, A. R.; Livage, C.; Férey, G.; Cheetham, A. K. *Chem. Commun.* **2004**, 368−369. (b) Gschwind, F.; Sereda, O.; Fromm, K. M. *Inorg. Chem.* **2009**, *48*, 10535−10547.
(24) Gao, S.; Yang, S.; Shu, J.; Zhang, S.; Li, Z.; Jiang, K. *J. Phys. Chem. C* **2008**, *112*, 19324−19328.
(25) Kumar, R. V.; Elgamiel, R.; Diamant, Y.; Gedanken, A.; Norwig, J. *Langmuir* **2001**, *17*, 1406−1410.
(26) Park, J. C.; Kim, J.; Kwon, H.; Song, H. *Adv. Mater.* **2009**, *21*, 803−807.
(27) Idota, Y.; Kubota, T.; Matsufuji, A.; Maekawa, Y.; Miyasaka, T. *Science* **1997**, *276*, 1395−1397.